

Traction Control for a Rocker-Bogie Robot with Wheel-Ground Contact Angle Estimation

Viboon Sangveraphunsiri and Mongkol Thianwiboon
Robotics and Automation Laboratory, Department of Mechanical Engineering
Faculty of Engineering, Chulalongkorn University,
Phayathai Rd. Pratumwan, Bangkok 10330, Thailand
E-Mail: Viboon.s@eng.chula.ac.th and kieng@eng.chula.ac.th

Abstract

A method for kinematics modeling of a six-wheel Rocker-Bogie mobile robot is described in detail. The forward kinematics is derived by using wheel Jacobian matrices in conjunction with wheel-ground contact angle estimation. The inverse kinematics is to obtain the wheel velocities and steering angles from the desired forward velocity and turning rate of the robot. Traction Control is also developed to improve traction by comparing information from onboard sensors and wheel velocities to minimize wheel slip. Finally, simulation of a small robot using rocker-bogie suspension has been performed and simulate in two conditions of surfaces including climbing slope and travel over a ditch.

Keywords: Rocker-Bogie Suspension / Traction Control / Slip Ratio

1. Introduction

The effectiveness of a wheeled mobile robot has been proven by NASA by sending a semi-autonomous rover "Sojourner" landed on Martian surface in 1997 [1]. Future field mobile robots are expected to traverse much longer distance over more challenging terrain than Sojourner, and perform more difficult tasks. Other examples of rough terrain applications for robotic can be found in hazardous material handling applications, such as explosive ordnance disposal, search and rescue.

Corresponding to such growing attention, the researches are varying from mechanical design, performance of the robot, control system, navigation systems, path planning, field test and so on.

However, there are very few concerning dynamics of the robot. This is because the field robots are considered too slow to encounter dynamic effect. And the high mobility of the robot, moving in 3 dimensions with 6 degrees of freedom (X, Y, Z, pitch, yaw, roll), makes the kinematics modeling a challenging task than the robots which move on flat and smooth surface (3 degrees of freedom : X, Y, rotation about Z axis).

In rough terrain, it is critical for mobile robots to maintain maximum traction. Wheel slip could cause the robot to lose control and trapped. Traction control for low-speed mobile robots on flat terrain has been studied by Reister and Unseren [2] using pseudo velocity to synchronize the motion of the wheels during rotation about a point. Sreenivasan and Wilcox [3] have

considered the effects of terrain on traction control by assume knowledge of terrain geometry, soil characteristics and real-time measurements of wheel-ground contact forces. However, this information is usually unknown or difficult to obtain directly. Quasi-static force analysis and fuzzy logic algorithm have been proposed for a rocker-bogie robot [4].

Knowledge of terrain geometry is critical to the traction control. A method for estimating wheel-ground contact angles using only simple on-board sensors has been proposed [5]. A model of load-traction factor and slip-based traction model has been developed [6]. The traveling velocity of the robot is estimated by measure the PWM duty ratio driving the wheels. Angular velocities of the wheels are also measured then compare with estimated traveling velocity to estimate the slip and perform traction control loop.

In this research work, the method to derive the wheel-ground contact angle estimation and kinematics modeling of a small six-wheel robot with Rocker - Bogie suspension are described. A traction control is proposed and integrated with the model then examined by simulation.

2. Rocker-Bogie Suspension

In this research, the computer model of the robot named "Lonotech 10" is built. Its dimensions are 480x640x480 mm³, consists of six wheels, three on each side. Four steering mechanisms are equipped to the front and rear wheels.

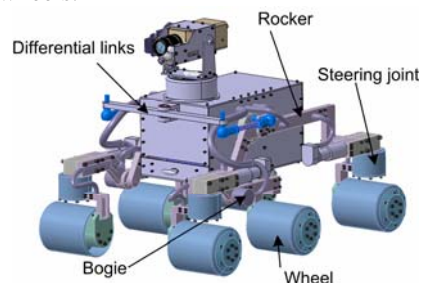


Figure 1. Lonotech 10

All independently actuated wheels are connected by the Rocker-Bogie suspension, a passive suspension that works well at low-velocity. This suspension consists of two rocker arms connected to the sides of the robot body.

At one end of each rocker is connected to pivot of the smaller rocker, the bogie, and the other end has a steerable wheel attached. Two wheels are attached to the end of these bogies. The rockers connected to the body via a differential link. This configuration maintains the pitch of the body equal to the average angle between the two rockers. This mechanism also provides an important mobility characteristic of the robot: one wheel can be lifted vertically while other wheels remain in contact with the ground.

3. Wheel-Ground Contact Angle Estimation

To formulate kinematics modeling for the mobile robot, the wheel-ground contact angles must be known. But it is difficult to make a direct measurement of these angles, a method for estimating the contact angles based on [5] is implemented to the rocker-bogie suspension in this section.

In kinematics modeling and contact angle estimation, we introduce the following assumptions.

- 1) Each wheel makes contact with the ground at a single point.
- 2) No side slip and rolling slip between a wheel and the ground.

Consider the left bogie on uneven terrain, the bogie pitch, μ_1 , is defined with respect to the horizon. The wheel center velocities, v_1 and v_2 , are parallel to the wheel-ground tangent plane. The distance between the wheel centers is L_B .

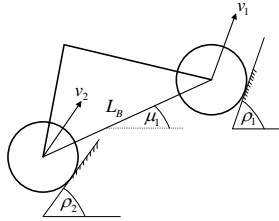


Figure 2. The left bogie on uneven terrain

The kinematics equations can be written as following

$$v_1 \cos(\rho_1 - \mu_1) = v_2 \cos(\rho_2 - \mu_1) \quad (1)$$

$$v_1 \sin(\rho_1 - \mu_1) - v_2 \sin(\rho_2 - \mu_1) = L_B \dot{\mu}_1 \quad (2)$$

Combining Equations (1) and (2):

$$\sin[(\rho_1 - \mu_1) - (\rho_2 - \mu_1)] = (L_B \dot{\mu}_1 / v_1) \cos(\rho_2 - \mu_1)$$

Define $a_1 = L_B \dot{\mu}_1 / v_1$, $b_1 = v_2 / v_1$

Contact angles of the wheel 1 and 2 are given by

$$\rho_1 = \mu_1 + \arcsin[(a_1^2 - b_1^2) / 2a_1] \quad (3)$$

$$\rho_2 = \mu_1 + \arcsin[(1 + a_1^2 - b_1^2) / 2a_1] \quad (4)$$

In order to compute the contact angle of the rear wheel, we need to know velocity of the bogie joint first.

Define r_{B_1} : rotation radius of the left bogie

$\dot{\mu}_1$: angular velocity of the left bogie

The velocity of the bogie joint can be written as:

$$v_{B_1} = r_{B_1} \dot{\mu}_1$$

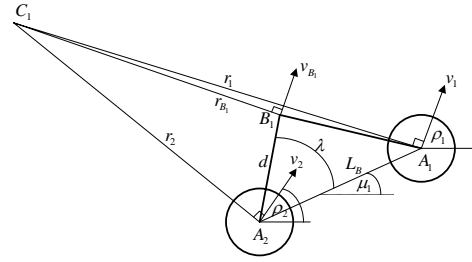


Figure 3. Instantaneous center of rotation of the left bogie

where $r_{B_1} = \sqrt{r_2^2 + d^2 - 2r_2 d \cos(90 + \rho_2 - \mu_1 - \lambda)}$

$$r_1 = L_B \sin(90 + \rho_2 - \mu_1) / \sin(\rho_1 - \rho_2)$$

$$r_2 = L_B \sin(90 - \rho_1 + \mu_1) / \sin(\rho_1 - \rho_2)$$

Consider Left Rocker, the rocker pitch, τ_1 , is defined with respect to the horizon direction. The distance between rear wheel center and bogie joint is L_R .

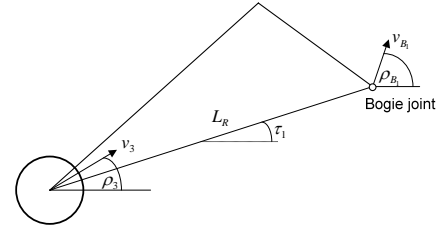


Figure 4. Left Rocker on an uneven terrain

Contact angles of the wheel 3 is

$$\rho_3 = \arccos[(v_{B_1} / v_3) \cos(\rho_{B_1} - \tau_1)] \quad (5)$$

In the same way, we repeated these procedures with the right side:

$$\rho_4 = \mu_2 + \arcsin[(a_2^2 - b_2^2) / 2a_2] \quad (6)$$

$$\rho_5 = \mu_2 + \arcsin[(1 + a_2^2 - b_2^2) / 2a_2] \quad (7)$$

$$\rho_6 = \arccos[(v_{B_2} / v_6) \cos(\rho_{B_2} - \tau_2)] \quad (8)$$

There are special cases that the contact angle cannot be estimated [5]. First occur when the robot is stationary. Pitch rates of the bogie and rocker cannot be computed. Then equations (3)-(5) do not yield a solution. Since a robot in a fixed configuration has an infinite set of contact angles. The second case occurs when the bogie is parallel to the surface and the front wheel encounter a vertical obstacle with respect to the surface.

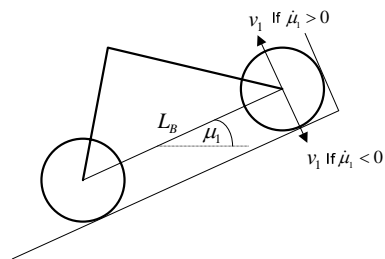


Figure 5. Left Bogie where $\cos \varepsilon_1 = 0$

However, by observation that v_2 is zero, equation (1) and (2) can be written as

$$v_1 \cos(\rho_1 - \mu_1) = 0 \quad (9)$$

$$v_1 \sin(\rho_1 - \mu_1) = L_B \dot{\mu}_1 \quad (10)$$

The variable ρ_2 is undefined since wheel 2 is stationary, and

$$\rho_1 = \mu_1 + \frac{\pi}{2} \text{sgn}(\dot{\mu}_1) \quad (11)$$

The last case occurs when ρ_1 is equal to ρ_2 . The pitch rate $\dot{\mu}_1$ is zero and ratio of v_2 and v_1 is unity. Then equations (3)-(5) have no solution. But it is easy to detect constant pitch rate from an inclinometer. If the bogie is on the flat terrain, the contact angles are equal to the pitch angle. In the case that pitch rate is zero temporary; we assume that the terrain profile varies slowly with respect to data sampling rate and use previously to estimate contact angle instead.

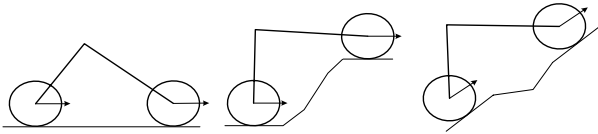


Figure 6. Left Bogie where $\dot{\mu}_1 = 0$ and $\frac{v_2}{v_1} = 0$

4. Forward Kinematics

We define coordinate frames as in Fig. 7 and 8. The subscripts for the coordinate frames are as follows: O : robot frame, D : differential joint, B_i : left and right bogie ($i=1,2$), S_i : steering of left front, left rear, right front and right rear wheels ($i=1,3,4,6$) and A_i : Axle of all wheels ($i=1-6$). Other quantities shown are steering angles ψ_i ($i=1,3,4,6$), rocker angle β , left and right bogie angle γ_1 and γ_2 .

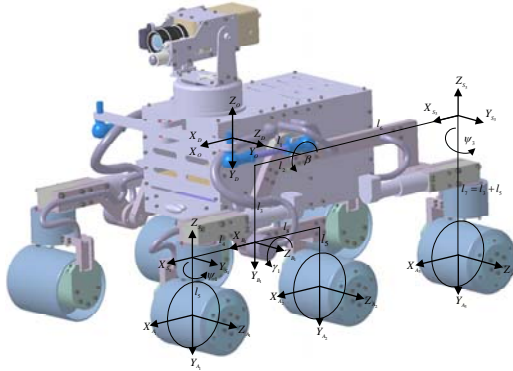


Figure 7. Left Coordinate frames

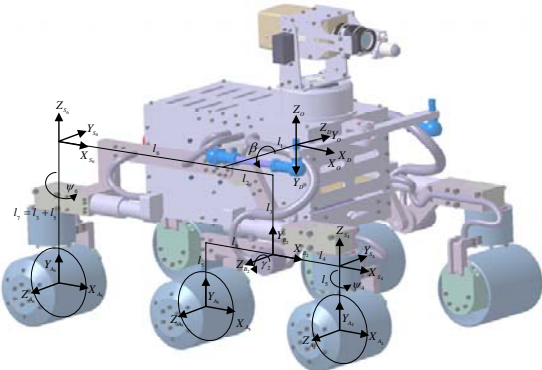


Figure 8. Right Coordinate frames

By following the Denavit-Hartenburg notation [7], the transformation matrix for coordinate i to j can be written as follows:

$$\mathbf{T}_{j,i} = \begin{bmatrix} C\Theta_j & -S\Theta_j C\alpha_j & S\Theta_j S\alpha_j & a_j C\Theta_j \\ S\Theta_j & C\Theta_j C\alpha_j & -C\Theta_j S\alpha_j & a_j S\Theta_j \\ 0 & S\alpha_j & C\alpha_j & d_j \\ 0 & 0 & 0 & 1 \end{bmatrix}$$

where Θ_j, α_j, a_j and d_j are the D-H parameters given for coordinate frame j . In this transformation, we have used the notation $C\Theta_j = \cos \Theta_j$ and $S\Theta_j = \sin \Theta_j$, etc.

The transformations from the robot reference frame (O) to the wheel axle frames (A_i) are obtained by cascading the individual transformations. For example, the transformations for wheel 1 are

$$\mathbf{T}_{O,A_1} = \mathbf{T}_{O,D} \mathbf{T}_{D,B_1} \mathbf{T}_{B_1,S_1} \mathbf{T}_{S_1,A_1}$$

In order to capture the wheel motion, we need to derive two additional coordinate frames for each wheel, contact frame and motion frame. Contact frame is obtained by rotating the wheel axle frame (A_i) about the z-axis followed by a 90 degree rotation about the x-axis. The z-axis of the contact frame (C_i) points away from the contact point as shown in Fig. 7.

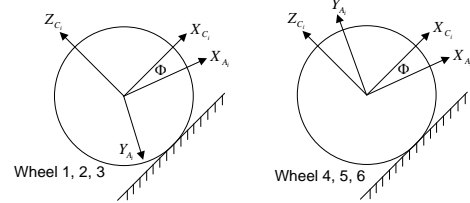


Figure 9. Contact Coordinate Frame

The transformation matrices for contact frame are derived using Z-X-Y Euler angle

$$\mathbf{T}_{A_i,C_i} = \begin{bmatrix} C p_i C r_i - S p_i S q_i S r_i & C r_i S p_i + C p_i S q_i S r_i & -C q_i S r_i & 0 \\ -C q_i S p_i & C p_i C q_i & S q_i & 0 \\ C r_i S p_i S q_i + C p_i C r_i & -C p_i C r_i S q_i + S p_i S r_i & C q_i C r_i & 0 \\ 0 & 0 & 0 & 1 \end{bmatrix}$$

where p_i, q_i and r_i are rotation angle about X, Y and Z respectively. $C p_i = \cos p_i$ and $S p_i = \sin p_i$, etc.

The wheel motion frame is obtained by translating along the negative z-axis by wheel radius (R_w) and translating along the x-axis for wheel roll ($R_w \theta_i$)

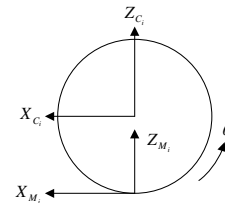


Figure 10. Wheel Motion Frame

The transformation matrices for all wheels can be written as follows:

$$\begin{aligned}\mathbf{T}_{O,M_1} &= \mathbf{T}_{O,D} \mathbf{T}_{D,B_1} \mathbf{T}_{B_1,S_1} \mathbf{T}_{S_1,A_1} \mathbf{T}_{A_1,C_1} \mathbf{T}_{C_1,M_1} \\ \mathbf{T}_{O,M_2} &= \mathbf{T}_{O,D} \mathbf{T}_{D,B_1} \mathbf{T}_{B_1,A_2} \mathbf{T}_{A_2,C_2} \mathbf{T}_{C_2,M_2} \\ \mathbf{T}_{O,M_3} &= \mathbf{T}_{O,D} \mathbf{T}_{D,S_3} \mathbf{T}_{S_3,A_3} \mathbf{T}_{A_3,C_3} \mathbf{T}_{C_3,M_3} \\ \mathbf{T}_{O,M_4} &= \mathbf{T}_{O,D} \mathbf{T}_{D,B_2} \mathbf{T}_{B_2,S_4} \mathbf{T}_{S_4,A_4} \mathbf{T}_{A_4,C_4} \mathbf{T}_{C_4,M_4} \\ \mathbf{T}_{O,M_5} &= \mathbf{T}_{O,D} \mathbf{T}_{D,B_2} \mathbf{T}_{B_2,A_5} \mathbf{T}_{A_5,C_5} \mathbf{T}_{C_5,M_5} \\ \mathbf{T}_{O,M_6} &= \mathbf{T}_{O,D} \mathbf{T}_{D,S_6} \mathbf{T}_{S_6,A_6} \mathbf{T}_{A_6,C_6} \mathbf{T}_{C_6,M_6}\end{aligned}$$

In order to obtain the wheel Jacobian matrices, the motion of the robot is express in the wheel motion frame, by applying the transformation $\dot{\mathbf{T}}_{\dot{o},O} = \mathbf{T}_{\dot{o},M_i} \dot{\mathbf{T}}_{M_i,O}$ and can be written in the following form as

$$\dot{\mathbf{T}}_{\dot{o},O} = \begin{bmatrix} 0 & -\dot{\phi} & \dot{p} & \dot{x} \\ \dot{\phi} & 0 & -\dot{r} & \dot{y} \\ -\dot{p} & \dot{r} & 0 & \dot{z} \\ 0 & 0 & 0 & 1 \end{bmatrix} \quad (12)$$

where ϕ = yaw angle of the robot
 p = pitch angle of the robot
 r = roll angle of the robot

Once the instantaneous transformations are obtained, we can extract a set of equations relating the robot's motion in vector form $[\dot{x} \ \dot{y} \ \dot{z} \ \dot{\phi} \ \dot{p} \ \dot{r}]^T$ to the joint angular rates. The results of the left and right front wheel are found to be

$$\begin{bmatrix} \dot{x} \\ \dot{y} \\ \dot{z} \\ \dot{\phi} \\ \dot{p} \\ \dot{r} \end{bmatrix} = \begin{bmatrix} A_i & 0 & B_i & C_i \\ D_i & 0 & E_i & F_i \\ G_i & 0 & H_i & I_i \\ 0 & 0 & 0 & J_i \\ 0 & -1 & -1 & 0 \\ 0 & 0 & 0 & K_i \end{bmatrix} \begin{bmatrix} \dot{\theta}_i \\ \dot{\beta} \\ \dot{\gamma}_i \\ \dot{\psi}_i \end{bmatrix} \quad i = 1,4 \quad (13)$$

The results of wheel 2 and 5 (the left and right middle wheel) are found to be

$$\begin{bmatrix} \dot{x} \\ \dot{y} \\ \dot{z} \\ \dot{\phi} \\ \dot{p} \\ \dot{r} \end{bmatrix} = \begin{bmatrix} A_i & 0 & B_i \\ C_i & 0 & 0 \\ D_i & 0 & E_i \\ 0 & 0 & 0 \\ 0 & -1 & -1 \\ 0 & 0 & 0 \end{bmatrix} \begin{bmatrix} \dot{\theta}_i \\ \dot{\beta} \\ \dot{\gamma}_i \end{bmatrix} \quad i = 2,5 \quad (14)$$

The results of wheel 3 and 6 (the left and right back wheel) are found to be

$$\begin{bmatrix} \dot{x} \\ \dot{y} \\ \dot{z} \\ \dot{\phi} \\ \dot{p} \\ \dot{r} \end{bmatrix} = \begin{bmatrix} A_i & 0 & B_i \\ C_i & 0 & D_i \\ E_i & 0 & F_i \\ 0 & 0 & G_i \\ 0 & -1 & 0 \\ 0 & 0 & H_i \end{bmatrix} \begin{bmatrix} \dot{\theta}_i \\ \dot{\beta} \\ \dot{\psi}_i \end{bmatrix} \quad i = 3,6 \quad (15)$$

where $\dot{\theta}$ is the angular velocity of the wheel, $\dot{\beta}$ is the rocker pitch rate, $\dot{\gamma}$ is the bogie pitch rate and $\dot{\psi}$ is the steering rate of the steerable wheel.

The parameters A_i to K_i in the matrices above can be easily derived in terms of wheel-ground contact angle (ρ_1, \dots, ρ_6) and joint angle (β, γ , and ψ). For example, the parameter A_1 of the front left wheel is

$$A_1 = \frac{1}{(-2 + S(2\rho_1))^2} [C(\beta + \gamma_1)(C\rho_1(C\psi_1 - S\psi_1) + S\rho_1 S\psi_1)(200 - 400C\rho_1 S\rho_1 + 200C^2\rho_1 S^2\rho_1)]$$

We will see that the 5th equation (5th row) does not contribute to any unknowns. It simply states that the change in pitch is equal to the change in the bogie and rocker angles. With the help of an installed inclinometer, \dot{p} can be sensed without knowledge of the rocker and bogie angles. Since only the \dot{p} , in equation (13) to (15), contains $\dot{\gamma}$ and $\dot{\beta}$, we can remove these for further consideration.

5. Inverse Kinematics

The purpose of inverse kinematics is to determine the individual wheel rolling velocities which will accomplish desired robot motion. The desired robot motion is given by forward velocity and turning rate. In this section, we will develop all 6 wheels rolling velocities with geometric approach to determine steering angle of steerable wheels.

5.1 Wheel Rolling Velocities

Consider forward kinematics of the front wheel (12), define the desired forward velocity is \dot{x}_d and desired heading angular rate is $\dot{\phi}_d$. The first and the fourth equation give

$$\begin{aligned}\dot{x}_d &= A_i \dot{\theta}_i + B_i \dot{\gamma}_i + C_i \dot{\psi}_i \\ \dot{\phi}_d &= J_i \dot{\psi}_i\end{aligned} \quad i = 1,3 \quad (16)$$

The rolling velocities of the front wheels can be written as

$$\dot{\theta}_i = (\dot{x}_d - B_i \dot{\gamma}_i - \frac{C_i}{J_i} \dot{\phi}_d) / A_i \quad i = 1,3 \quad (17)$$

Similarly, the rolling velocities of the middle wheels can be written as

$$\dot{\theta}_i = (\dot{x}_d - B_i \dot{\gamma}_i) / A_i \quad i = 2,5 \quad (18)$$

Finally the rolling velocities of the back wheels can be written as

$$\dot{\theta}_i = (\dot{x}_d - \frac{B_i}{G_i} \dot{\phi}_d) / A_i \quad i = 3,6 \quad (19)$$

5.2 Steering Angles

Center of rotation is estimated based on two non-steerable middle wheels. This turning center will be used to determine the steering angles of the four corner wheels. From Fig. 7 and 8, we can derive coordinate of the wheel centers respect to the robot reference frame as follows:

$$\begin{aligned}
 x_{C1} &= l_2 \cos \beta + l_3 \sin \beta + l_4 \cos(\beta - \gamma_1) + l_5 \sin(\beta - \gamma_1) \\
 x_{C2} &= l_2 \cos \beta + l_3 \sin \beta - l_8 \cos(\beta - \gamma_1) + l_5 \sin(\beta - \gamma_1) \\
 x_{C3} &= -l_6 \cos \beta + (l_3 + l_5) \sin \beta \\
 x_{C4} &= l_2 \cos(-\beta) - l_3 \sin(-\beta) + l_4 \cos(-\beta + \gamma_2) + l_5 \sin(-\beta + \gamma_2) \\
 x_{C5} &= l_2 \cos(-\beta) - l_3 \sin(-\beta) - l_8 \cos(-\beta + \gamma_2) + l_5 \sin(-\beta + \gamma_2) \\
 x_{C6} &= -l_6 \cos(-\beta) - (l_3 + l_5) \sin \beta
 \end{aligned}$$

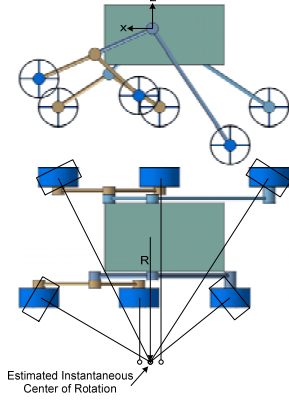


Figure 11. Instantaneous Center of Rotation

From Fig. 11, the instantaneous center of rotation can be estimated by average the x position of the middle wheels. The distance in Z axis is neglected because there is only 1 degree of freedom per each steering. If the wheel's axis is steered to intersect with the center of rotation on the X axis, the angle in Z direction is coupled and cannot be controlled.

Using the estimated center of rotation, the desired steering angle for each steerable wheel can be determined. Define R is a turning radius, x_R is the distance in X-direction of the center of rotation with respect to the robot reference frame. l_1 is the distance from the robot reference frame to steering joint in Y-direction (see figure 7 and 8). The desired steering angles are

$$\begin{aligned}
 \psi_1 &= \arctan[(x_{C1} - x_R)/(R - l_1)] && \text{for wheel 1} \\
 \psi_3 &= \arctan[(x_{C3} - x_R)/(R - l_1)] && \text{for wheel 3} \\
 \psi_4 &= \arctan[(x_{C4} - x_R)/(R + l_1)] && \text{for wheel 4} \\
 \psi_6 &= \arctan[(x_{C6} - x_R)/(R + l_1)] && \text{for wheel 6}
 \end{aligned}$$

6. Traction Control

In section 4 and 5, we assume that there is no side slip and rolling slip between wheel and ground. Then slip must be minimizing to guarantee accuracy of the kinematics model. The slip ratio S , of each wheel is defined as follows [6]:

$$S = \begin{cases} (r\dot{\theta}_w - v_w)/r\dot{\theta}_w & (r\dot{\theta}_w > v_w : \text{accelerating}) \\ (r\dot{\theta}_w - v_w)/v_w & (r\dot{\theta}_w < v_w : \text{decelerating}) \end{cases} \quad (30)$$

- where r = radius of the wheel
- θ_w = rotating angle of the wheel
- $r\dot{\theta}_w$ = wheel circumference velocity
- v_w = traveling velocity of the wheel

S is positive when the robot is accelerating and negative when decelerating.

From the slip ratio, a robot can travel stably when the slip ratio is around 0 and will be stuck when the ratio is around 1. To gain maximum traction, we must keep the slip ratio at a small as possible.

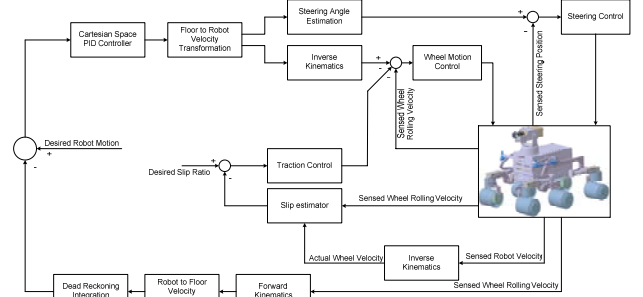


Figure 12. Robot Control Schematic

By measuring of the wheel angles with information from the accelerometer, we can minimize slip so that the traction of the robot is improved. The control problem is to control the slip S to a desired set point S_d that is either constant or commanded from a higher-level control system. The feedback value \hat{S} is computed from a slip estimator. To complete the estimation of the slip, we need the rolling velocity and the traveling velocity of the wheels, ω and v_w . Rolling velocity of the wheels is easily obtained from encoders which installed in all wheels. Traveling velocity of the wheel can be computed from robot velocity by using data from onboard accelerometer.

The robot velocity can be obtained by integrating the accelerometer signal. Then use this value as an input to the inverse kinematics to compute the rolling velocities of all wheels. Then multiply by wheel radius, we can obtain the traveling velocity of the wheels.

7. Experiment

The traction control system was verified by simulation on Visual Nastran 4D. In Fig. 12, the robot climbs up a 30-degree slope, with coefficient of friction about 0.5.

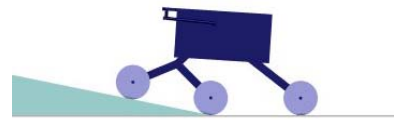


Figure 13. Robot climbing up a slope

As a result, in case without control, the robot was running at 55 mm/s, then the front wheels touched the slope at $t=0.5$ sec. and begin to climb up. Robot velocity measured in reduced to 25 mm/s. But the robot can continue to climb until the middle wheels touch the slope at $t=9$ sec. The velocity reduced to nearly zero.

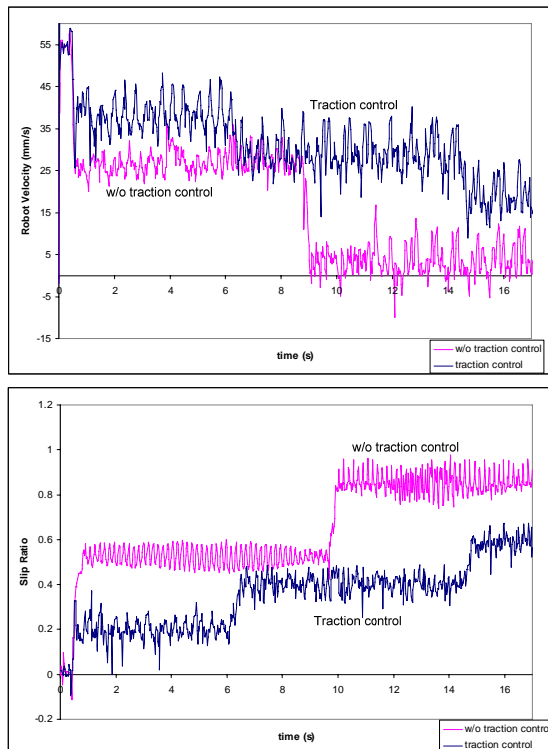


Figure 14. Velocity and Slip ratio when climbing up 30 degrees slope

In case with control, the sequence was almost the same until $t = 0.5$ sec. The velocity reduced to approximately 35 mm/s when the front wheels touched the slope. At $t = 6$ sec., the middle wheels touched the slope and velocity reduced to about 28 mm/s. And both rear wheels begin to climb up the slope at $t = 15$ sec. with velocity approximately 20m/s.



Figure 15. Traversing over a ditch

In Fig. 15, the robot traversed over a ditch, which has 32 mm depth and 73 mm width with coefficient of friction about 0.5. The robot was commanded to move at 55 mm/s, and then the front wheels went down the ditch at $t = 0.5$ sec. The velocity of the robot increased temporary and begin to climb up when front wheels touch the up-edge of the ditch. But the wheels slipped with the ground and failed to climb up. Then the slip ratio went up to 1 ($S=1$), the robot has stuck and the velocity decreased about zero at $t = 1.5$ sec.

With traction control, after the front wheels went down the ditch, the slip ratio was increased. Then the controller tried to decelerate to decrease the slip ratio. When the slip ratio was around 0.5, the robot continued to climb up. Until $t = 4.5$ sec., both of the front wheels went up the ditch completely and the robot velocity increased to the 55 mm/s as commanded.

At $t = 6$ sec., the middle wheels went down the

ditch. The robot velocity also increased temporary and back to 55 mm/s again when the middle wheels went up completely. The last two wheels went down the ditch at $t = 13$ sec. and the sequence was repeated in the same way as front and middle wheels.

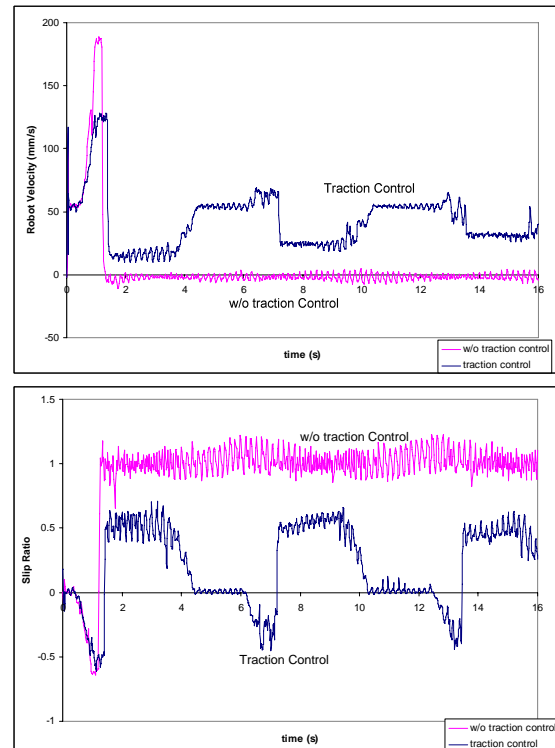


Figure 16. Velocity and Slip ratio when traversing over a ditch

7. Conclusion

In this research, the wheel-ground contact angle estimation has been presented and integrated into a kinematics modeling. Unlike the available methods that applicable to the robots operating on flat and smooth terrain, the proposed method uses the Denavit-Hartenburg notation like a serial link robot, due to the rocker-bogie suspension characteristics. The steering angle is estimated by using geometric approach.

A traction controller is proposed based on the slip ratio. The slip ratio is estimated from wheel rolling velocities and the robot velocity. The traction control strategy is to minimize this slip ratio. So the robot can traverse over obstacle without being stuck.

The traction control strategy is verified in the simulation with two conditions. Climbing up the slope and moving over a ditch with coefficient of friction 0.5. The robot velocity and slip ratio are compared between using traction control and without using traction control system.

References

- [1] JPL Mars Pathfinder. February 2003. Available from: <http://mars.jpl.nasa.gov/MPF>
- [2] D.B.Reister, and M.A.Unseren, "Position and Constraint force Control of a Vehicle with Two or More Steerable Drive Wheels", IEEE Transaction on

- Robotics and Automation, page 723-731, Volume 9, 1993.
- [3] S.Sreenivasan, and B.Wilcox, "Stability and Traction control of an Actively Actuated Micro-Rover", Journal of Robotic Systems, 1994.
 - [4] H.Hacot, "Analysis and Traction Control of a Rocker-Bogie Planetary Rover", M.S. Thesis, Massachusetts Institute of Technology, Cambridge, MA, 1998.
 - [5] K.Iagnemma, and S.Dubowsky, "Mobile Robot Rough-Terrain Control (RTC) for Planetary Exploration", Proceedings of the 26th ASME Biennial Mechanisms and Robotics Conference, Baltimore, Maryland, 2000.
 - [6] K.Yoshida, H.Hamano: Motion Dynamics of a Rover with Slip-Based Traction Model, Proceeding of 2002 IEEE International Conference on Robotics and Automation (2002)
 - [7] John J. Craig, "Introduction to Robotics Mechanics and Control", Second Edition, Addison-Wesley Publishing Company, 1989.
 - [8] M.Thianwiboon, V.Sangveraphunsiri, and R.Chancharoen, "Rocker-Bogie Suspension Performance", Proceeding of the 11th International Pacific Conference on Automotive Engineering, 2001.